



THE UNIVERSITY *of* EDINBURGH

## Edinburgh Research Explorer

### Genetic background modifies vulnerability to glaucoma related phenotypes in Lmx1b mutant mice

**Citation for published version:**

Tolman, NG, Balasubramanian, R, Macalinao, DG, Kearney, AL, MacNicoll, KH, Montgomery, CL, de Vries, WN, Jackson, IJ, Cross, S, Kizhatil, K, Nair, KS & John, SWM 2021, 'Genetic background modifies vulnerability to glaucoma related phenotypes in Lmx1b mutant mice', *Disease Models and Mechanisms*.  
<https://doi.org/10.1242/dmm.046953>

**Digital Object Identifier (DOI):**

[10.1242/dmm.046953](https://doi.org/10.1242/dmm.046953)

**Link:**

[Link to publication record in Edinburgh Research Explorer](#)

**Document Version:**

Peer reviewed version

**Published In:**

Disease Models and Mechanisms

**General rights**

Copyright for the publications made accessible via the Edinburgh Research Explorer is retained by the author(s) and / or other copyright owners and it is a condition of accessing these publications that users recognise and abide by the legal requirements associated with these rights.

**Take down policy**

The University of Edinburgh has made every reasonable effort to ensure that Edinburgh Research Explorer content complies with UK legislation. If you believe that the public display of this file breaches copyright please contact [openaccess@ed.ac.uk](mailto:openaccess@ed.ac.uk) providing details, and we will remove access to the work immediately and investigate your claim.



1 **Genetic background modifies vulnerability to glaucoma related phenotypes in *Lmx1b* mutant**  
2 **mice**

3 Tolman NG<sup>1,2,3</sup>, Balasubramanian R<sup>1</sup>, Macalinao DG<sup>3</sup>, Kearney AL<sup>3</sup>, MacNicol KH<sup>3</sup>, Montgomery, CL<sup>1</sup>,  
4 de Vries, WN<sup>3</sup>, Jackson IJ<sup>4</sup>, Cross SH<sup>4</sup>, Kizhatil K<sup>3</sup>, Nair KS<sup>5</sup>, John SWM<sup>1,3</sup>

5 <sup>1</sup> Howard Hughes Medical Institute, Department of Ophthalmology, Columbia University Medical  
6 Center, and Zuckerman Mind Brain Behavior Institute, New York, NY, USA

7 <sup>2</sup> Graduate School of Biomedical Sciences, Tufts University School of Medicine, Boston, MA 02115,  
8 USA

9 <sup>3</sup>The Jackson Laboratory, Bar Harbor, Maine 04609, USA

10 <sup>4</sup>MRC Human Genetics Unit, MRC IGMM, University of Edinburgh, Edinburgh, United Kingdom.

11 <sup>5</sup>Departments of Ophthalmology and Anatomy, School of Medicine, UCSF, San Francisco, CA, 94143,  
12 USA

13 **Abstract**

14 Variants in the LIM homeobox transcription factor 1-beta gene (*LMX1B*) predispose individuals to  
15 elevated intraocular pressure (IOP), a key risk factor for glaucoma. However, the effect of *LMX1B*  
16 mutations varies widely between individuals. To better understand mechanisms underlying LMX1B-  
17 related phenotypes and individual differences, we backcrossed the *Lmx1b*<sup>V265D</sup> (also known as  
18 *Lmx1b*<sup>lcst</sup>) allele onto the C57BL/6J (B6), 129/Sj (129), C3A/BLiA-*Pde6b*<sup>+</sup>/J (C3H), and DBA/2J-*Gpnmb*<sup>+</sup>  
19 (D2-G) mouse strain backgrounds. Strain background had a significant effect on the onset and severity  
20 of ocular phenotypes in *Lmx1b*<sup>V265D/+</sup> mutant mice. Mice of the B6 background were the most  
21 susceptible to developing an abnormal IOP distribution, severe anterior segment developmental  
22 anomalies (including malformed eccentric pupils, iridocorneal strands, and corneal abnormalities) and  
23 glaucomatous nerve damage. In contrast, *Lmx1b*<sup>V265D</sup> mice of the 129 background were the most  
24 resistant to developing anterior segment abnormalities, had less severe IOP elevation than B6 mutants  
25 at young ages, and showed no detectable nerve damage. To identify genetic modifiers of susceptibility  
26 to *Lmx1b*<sup>V265D</sup>-induced glaucoma-associated phenotypes, we performed a mapping cross between mice  
27 of the B6 (susceptible) and 129 (resistant) backgrounds. We identified a modifier locus on  
28 Chromosome 18, with the 129 allele(s) substantially lessening severity of ocular phenotypes, as  
29 confirmed by congenic analysis. By demonstrating a clear effect of genetic background in modulating  
30 *Lmx1b*-induced phenotypes, providing a panel of strains with different phenotypic severities, and  
31 identifying a modifier locus, this study lays a foundation for better understanding the roles of LMX1B in  
32 glaucoma with the goal of developing new treatments.

### 33 Introduction

34 Glaucoma is a group of complex disorders that share a characteristic pattern of visual field deficits and  
35 retinal ganglion cell degeneration. It is a leading cause of blindness worldwide affecting 80 million  
36 people (Quigley and Broman, 2006). Important risk factors for glaucoma include elevated intraocular  
37 pressure (IOP), genetics, and advanced age. Lowering IOP to a safe level is the only available  
38 treatment (Weinreb et al., 2014). The aqueous humor (AqH) drainage tissues, including the Schlemm's  
39 canal (SC) and trabecular meshwork (TM), have a key role in controlling IOP (Fautsch and Johnson,  
40 2006). Resistance to AqH drainage from the eye through the SC and TM is important in determining  
41 IOP. However, the mechanisms underlying dysfunctional AqH drainage and subsequent IOP elevation  
42 require additional characterization. A majority of glaucoma cases are attributed to primary open angle  
43 glaucoma (POAG), where IOP elevation lacks an obvious physical cause (Quigley and Broman, 2006).  
44 Recently, genome wide association studies (GWAS) have improved understanding of the genetic basis  
45 of POAG by implicating more than 70 loci (Bonnemaijer et al., 2018; Choquet et al., 2018; Choquet et  
46 al., 2020; Genetics of Glaucoma in People of African Descent et al., 2019; Khawaja et al., 2018;  
47 MacGregor et al., 2018; Taylor et al., 2019; Youngblood et al., 2019). Research that defines how these  
48 genes affect IOP is expected to yield new drug targets and improved treatments for lowering IOP  
49 (Choquet et al., 2020).

50 The LIM homeobox transcription factor 1-beta (*LMX1B*) gene was associated with elevated IOP and  
51 POAG through genome wide association studies (GWAS) and has been validated in multiple  
52 populations (Choquet et al., 2018; Gao et al., 2018; Gharahkhani et al., 2018; Khawaja et al., 2018;  
53 MacGregor et al., 2018; Shiga et al., 2018). Prior to GWAS, dominant mutations in *LMX1B* were  
54 identified to cause nail-patella syndrome (NPS) (Chen et al., 1998; Dreyer et al., 1998; Vollrath et al.,  
55 1998). NPS is a developmental disorder with characteristic symptoms including nail dysplasia and  
56 abnormally developed limb structures (Farley et al., 1999; Sweeney et al., 2003). Within NPS patients,  
57 20-30% develop elevated IOP and POAG, a prevalence that is significantly higher than in the general  
58 population (Mimiwati et al., 2006; Sweeney et al., 2003). Apart from POAG, there are a wide range of  
59 ocular phenotypes reported in NPS patients including developmental iris, corneal, and pupillary  
60 abnormalities and congenital glaucoma (Lichter et al., 1997; Sawamura et al., 2014; Spitalny and  
61 Fenske, 1970). Importantly, there are striking differences in onset and severity of phenotypes between  
62 patients that inherit the same *LMX1B* variant (Knoers et al., 2000; McIntosh et al., 2005; Sweeney et  
63 al., 2003). Thus, it is likely that genetic background modulates the risk of developing specific disease  
64 phenotypes in patients with *LMX1B* variants. Identifying genetic modifiers of *LMX1B*-related



phenotypes will be important in understanding risk of glaucoma and is expected to provide novel mechanistic information on the etiology of IOP elevation.

Based on high sequence homology, mice have been used to understand the biological role of *LMX1B* in several tissues (McIntosh et al., 2005). Previous work in mice has shown that *LMX1B* is required for the development and function of AqH drainage tissue including the TM (Liu and Johnson, 2010; Pressman et al., 2000). Mice with dominant point mutations in *Lmx1b* recapitulate several phenotypes found in humans with *LMX1B* variants. One important mutation causes a valine to aspartic acid substitution (*Lmx1b*<sup>V265D</sup>, also known as *Lmx1b*<sup>lcst</sup>) in the transcription factor's homeodomain, disrupting its ability to bind DNA (Cross et al., 2014). Mice heterozygous for *Lmx1b*<sup>V265D/+</sup> develop elevated IOP and glaucomatous neurodegeneration (Cross et al., 2014). Previous reports show *Lmx1b* heterozygous null alleles do not cause glaucoma in mice (Cross et al., 2014; Pressman et al., 2000). Importantly, the *Lmx1b*<sup>V265D</sup> allele is dominant negative and causes a different range and severity of abnormal phenotypes compared to a heterozygous null allele (Cross et al., 2014). *Lmx1b*<sup>V265D</sup> mice present with several additional ocular phenotypes including abnormal SC and TM, congenital defects of the iris such as iridocorneal strands, abnormally open pupils, and corneal phenotypes including corneal opacities, corneal neovascularization, and corneal scarring (Cross et al., 2014). Congenital abnormalities of the iris, cornea, and pupil have also been observed in a subset of NPS patients (Beals and Eckhardt, 1969; Bennett et al., 1973; Lichter et al., 1997; Spitalny and Fenske, 1970; Sweeney et al., 2003). Based on these phenotypic similarities, *Lmx1b*<sup>V265D</sup> mutant mice are a valuable model for determining mechanisms and modifiers of ocular disease phenotypes that may affect humans with *LMX1B* variants.

Given the phenotypic variation between individuals with the same *LMX1B* variant (McIntosh et al., 2005), we expected to find differences in glaucoma-associated ocular phenotypes between different genetically diverse mouse strains with the *Lmx1b*<sup>V265D</sup> allele. Here, we characterized the ocular effects of the *Lmx1b*<sup>V265D</sup> allele on four different mouse strain backgrounds. Our results show that strain background significantly affects the onset and progression of glaucoma-related phenotypes in *Lmx1b*<sup>V265D/+</sup> mice including IOP elevation and glaucomatous neurodegeneration. Based on this, we performed a gene mapping experiment between the most susceptible and resistant strain backgrounds and identified a modifier locus on Chromosome 18.

## Materials and Methods

### Animal husbandry and ethics statement

The *Lmx1b*<sup>V265D</sup> mutation was discovered in an ENU mutagenesis screen (Cross et al., 2014; Thaung et al., 2002). It is formally named the *lcst* (iridocorneal strands) allele, but we refer to it based on the protein level change V265D. Briefly, ENU-mutagenized Balb/cAnN (MRC Harwell, Oxfordshire, UK) were crossed to C3H/HeN mice (MRC Harwell, Oxfordshire, UK), and their offspring were screened (Thaung et al., 2002). Mice carrying the *lcst* mutation were crossed to C57BL/6J for gene mapping, and sequencing of the *Lmx1b* gene identified the V265D mutation (Cross et al., 2014; Thaung et al., 2002). These mice were then backcrossed to the C57BL/6J (Stock# 000664), DBA/2J-*Gpnmb*<sup>+</sup>/SjJ (Stock# 007048), C3A/BLiA-*Pde6b*<sup>+</sup>/J (Stock# 001912) and 129/Sj (Stock# 003884) for 8-10 generations. To determine if a tyrosinase deficient background exacerbated phenotypic severity, *Lmx1b*<sup>V265D</sup> was also backcrossed to the BALB/cJ (Stock# 000651) background for 6-8 generations and mice analyzed at 3 to 6 months of age. All experimental mice were backcrossed at least 6 generations. The 129/Sj strain was created from mice carrying a heterozygous knockout mutation generated in TL1 ES cells and maintained on a 129S6/SvEvTac background. We obtained this strain and selected mice without the heterozygous knockout mutation for inbreeding. Genotyping evidence suggests our 129/Sj strain contains large regions aligning to both 129S6/SvEvTac and 129S1/SvImJ respectively but is genetically distinct to any other 129 substrains (data not shown). DBA/2J, C3A/BLiA-*Pde6b*<sup>+</sup>/J, and 129/Sj mice were maintained on NIH 31 (6% fat) diet. To avoid obesity, C57BL/6J (B6) mice were maintained on NIH 31 diet (4% fat) diet and HCl acidified water (pH 2.8-3.2). Early studies showed that the minor difference in fat content did not affect the phenotypes. Mutant and control littermates were housed together with Alpha-dri bedding in cages covered with polyester filters. Cages were maintained in an environment kept at 21°C with a 14-hour light: 10-hour dark cycle. All mice were treated in accordance with the Association for Research in Vision and Ophthalmology's statement on the use of animals in ophthalmic research. The Institutional Animal Care and Use Committee of The Jackson Laboratory approved all experimental protocols.

### Genotyping of the *Lmx1b* allele

*Lmx1b*<sup>V265D</sup> and *Lmx1b*<sup>+</sup> genotypes were determined using an allele-specific PCR protocol. Genomic DNA was PCR amplified with forward primer specific to the V265D allele 5'-TCAGCGTGC GTGTGGTCCTGGA-3', a forward primer specific to the wild type allele 5'-GACATTGGCAGCAGAGACAGGCCGAGGCGTGC GTGTGGTCCATGT-3', and the reverse primer 5'-ACACAAGCCTCTGCCTCCTT-3'. Genomic DNA was PCR amplified using the following program; 1) 95°C for 2 minutes, 2) 95°C for 15 seconds, 3) 57 °C for 20 seconds, 4) 72 °C for 30 seconds, 5) repeat steps 2-4 35 times, 6) 72°C for seven minutes. 5 µl of sample was run on a 3% agarose gel. The wild type allele amplifies a 175 base pair fragment and the V265D allele amplifies a 152 base pair fragment.

128 Although we used these primers in this study, mismatches exist in some of them compared to reference  
129 sequence. We have subsequently confirmed that they provided accurate genotypes compared to  
130 Sanger sequencing. Reference matched primer sequences are 5'-TCAGCGTGCGTGTGGTCCAGGA-  
131 3' (V265D forward primer), 5'- GACATTGGCAGCAGAGACAGGCCTCAGCGTGCGTGTGGTCCAGGT-  
132 3' (wild type forward primer), and 5'-ACACAAGGCTCTGCCTCCTT-3' (reverse primer).

### 133 **Quantitative PCR (qPCR)**

134 RNA was isolated from ocular anterior segment tissues (except the lens) of B6, D2, and 129 inbred  
135 strains at 4 months of age (2 eyes pooled per sample). RNA was isolated using the RNeasy Mini Kit  
136 (Qiagen) according to the manufacturer's protocols. Total RNA was reverse transcribed using the high  
137 capacity cDNA Reverse Transcription kit (Applied Biosystems). Relative mRNA levels were determined  
138 by using the SYBR<sup>TM</sup> Green PCR Master Mix (Applied Biosystems) according to the manufacturer's  
139 instructions. For each reaction 400ng (anterior segment) of total RNA was used as input for reverse  
140 transcription, and 10ng of cDNA was used for qPCR. Primers used for *Lmx1b* were forward 5'  
141 GAGCAAAGATGAAGAAGCTGGC 3' and reverse 5' CTCCATGCGGCTTGACAGAA 3' [previously  
142 published in (Wever et al., 2019)]. Primers for *Gapdh* were forward 5'  
143 CGACTTCAACAGCAACTCCCACTCTTCC 3' and reverse 5'  
144 TGGGTGGTCCAGGGTTTCTTACTCCTT 3'. Quantitative PCR (qPCR) data was analyzed using the  
145 delta-delta Ct method. Results were statistically analyzed using Student's *t*-test. Graphs represent the  
146 fold change relative to B6 background expression (n= 3 for each strain).

### 147 **Slit-lamp examination**

148 Anterior eye tissues were examined approximately every 3 months between 2-13 months of age using  
149 a slit-lamp biomicroscope and photographed with a 40x objective lens. Phenotypic evaluation included  
150 iris structure, pupillary abnormalities, generalized corneal haze, corneal opacity, corneal keratopathy,  
151 hyphaema, hypopyon, corneal pyogenic granuloma, vascularized scarred cornea, buphthalmos,  
152 cataracts, and deepening of the anterior chamber. A subset of phenotypes that were common in  
153 *Lmx1b*<sup>V265D/+</sup> mice (anterior chamber deepening, pupillary abnormalities, corneal haze, and corneal  
154 opacity) were characterized and graded based on a semiquantitative scale of either phenotype being  
155 not present, mild, moderate, or severe in presentation (Table 1). Detailed examination of typically 40  
156 eyes from each strain and genotype at 4, 7, and 11 months of age was performed, except for the C3H  
157 background at 7 months where 12 mutant eyes and 14 WT eyes were examined. C3H mice at 4  
158 months were examined but no phenotypes were graded. We found no sex difference in onset and  
159 severity of the phenotypes. Therefore, we combined both sexes in our analyses, with all cohorts

including balanced numbers of male and female mice. Groups were compared pairwise by Fisher's exact test.

## **IOP measurement**

IOP was measured using the microneedle method as previously described in detail (John et al., 1997; Savinova et al., 2001). Briefly, mice were acclimatized to the procedure room and anesthetized via an intraperitoneal injection of a mixture of ketamine (99 mg/kg; Ketlar, Parke-Davis, Paramus, NJ) and xylazine (9 mg/kg; Rompun, Phoenix Pharmaceutical, St. Joseph, MO) immediately prior to IOP assessment, a procedure that does not alter IOP in the experimental window (Savinova et al., 2001). IOP values were grouped by mouse age. IOPs measured at 3 to 5.9 months of age were grouped into the young timepoint (3-6mo), 6 to 8.9 months were grouped into the intermediate timepoint (6-9mo), and mice 9 to 11.9 months were grouped into the older timepoint (9-12mo). *Lmx1b*<sup>V265D/+</sup> and WT IOP distributions did not meet the assumption of equal variance by Levene's test. Therefore, we compared individual groups by two-tailed Welch's *t*-test. In mice, IOP elevation caused by different mutations (including mutations in human glaucoma genes) is often accompanied by both an upward and a downward spread of values. This is due to complex effects including ocular stretching, perturbations of diurnal regulation and ciliary body dysfunction or atrophy (Chang et al., 2001; John et al., 1998). This spreading effect was strong in our current study and especially so for the V265D allele (likely exacerbated by their weakened/ expandable corneas and corneal ulceration with perforation in some mice - see text). Thus, to examine the magnitude of IOP dysregulation in *Lmx1b*<sup>V265D/+</sup> eyes, we used the absolute value of the difference from the WT mean of each measurement (calculated by subtracting each mutant or WT value from the WT mean of the matching strain background and age). Distributions of these values were plotted and, as they also failed the assumption of equal variance between groups, were compared statistically by two-tailed Welch's *t*-test. To further visualize the change in variance between *Lmx1b*<sup>V265D/+</sup> and WT groups, we binned IOP values into four categories (<10mmHg, 10-19.9mmHg, 20-29.9 mmHg, and ≥30mmHg). The percentage of IOP values within each category was compared across experimental groups by Fisher's exact test. We measured IOP of at least 30 eyes per group (age, genotype, and strain background) except for C3H background mice at 6-8 months where n= 20 mutant and 13 WT. All cohorts included balanced number of male and female mice. During each IOP measurement period, eyes of independent wild-type B6 mice were assessed in parallel with experimental mice as a methodological control to ensure proper calibration and equipment function.

## **Ocular histological analysis**

191 Enucleated eyes were fixed for plastic sectioning (0.8% paraformaldehyde and 1.2% glutaraldehyde in  
192 0.08 M phosphate buffer (pH 7.4) as previously described in detail (John et al., 1998). Serial sagittal  
193 sections were collected, stained with hematoxylin and eosin, and analyzed for pathologic alterations at  
194 3 months of age. For analysis of angle morphology relevant to drainage function, we used a previously  
195 validated grading scheme to determine the degree of angle closure due to adhesions/malformations  
196 that block drainage (Libby et al., 2003). The lower the total score the more extensively an angle is open  
197 around the circumference of any eye, while the higher the score the more closed it is. Briefly, we  
198 evaluated 24 similarly spaced angle regions from of each eye including the peripheral, mid-peripheral,  
199 and central ocular regions. For a few WT eyes, only 15 to 22 angle locations were scored due to  
200 regional processing artifacts. Angle scores for such eyes were normalized to the others for direct  
201 comparison. Each angle was graded based on the extent of angle blockage by attachment of the iris to  
202 the trabecular meshwork and cornea as previously reported (Libby et al., 2003) (0 = normal, iris and  
203 ciliary body join at iris root with no adhesion to the TM or cornea, 1 = iris attached to very posterior  
204 portion of TM so that most of the TM/angle is open and accessible for drainage, 2 = iris attached to TM  
205 for up to three quarters of the extent of TM, 3 = iris covers entire TM and extends just into peripheral  
206 cornea indicating a completely closed angle region, 4 = iris covers TM and adhesion extends further  
207 onto cornea). The final angle score is the sum of values for each angle location. The minimum possible  
208 score is 0, reflecting a completely normal, fully-open angle at all locations. A score of 24, would indicate  
209 that either the angle is completely open for at least 75% of the assessed circumference with minor  
210 abnormalities in the remaining 20%, or that an angle is open for even more of its circumference with  
211 focal occurrence or more severe abnormalities. The maximum score is 96 (4 X 24) reflects a completely  
212 closed angle at all locations with extensive attachment of the iris to the peripheral cornea. A score of 72  
213 (3 x 24) also reflects a completely closed angle as the iris completely covers the TM at all assessed  
214 locations in such eyes. The samples were intermixed, and the observers were not aware of the *Lmx1b*  
215 genotype or genetic background during the grading. Two observers, masked to sample identity as well  
216 as each other, graded the eyes. The score assigned by each observer agreed >96% of the time and  
217 never disagreed by more than 1 grade. Disagreements involved regions with abnormalities at the  
218 border of two grades and differences were resolved by consensus agreement when still masked to  
219 sample identity. The summed grade of all the examined angles from each mouse is plotted. Because  
220 the data was discretized, groups were statistically compared by Mann-Whitney U test. Each group  
221 contained balanced numbers of male and female mice. We analyzed 5-7 eyes, with a median of 6 eyes  
222 of each genotype for both the 129 and B6 strains.

## 223 **Optic nerve assessment**

224 Intracranial portions of optic nerves were dissected, processed, and analyzed as previously described  
225 (Howell et al., 2007; Howell et al., 2012; Nair et al., 2016; Williams et al., 2017). Briefly, optic nerve  
226 cross-sections were stained with para-phenylenediamine (PPD) and examined for glaucomatous  
227 damage. PPD stains all myelin sheaths of a healthy axon, but differentially darkly stains the myelin  
228 sheaths and the axoplasm of sick or dying axons. This allows for the sensitive detection and  
229 quantification of axon damage and loss. Optic nerves were prepared for analysis with a 48h fixation in  
230 0.8% paraformaldehyde and 1.2% glutaraldehyde in 0.08M phosphate buffer (pH 7.4) at 4°C followed  
231 by overnight treatment in osmium tetroxide at 4°C. Nerves were washed twice for 10 minutes on 0.1 M  
232 phosphate buffer, once in 0.1 M sodium-acetate buffer and dehydrated in graded ethanol  
233 concentrations. Tissues were then embedded in Embed 812 resin (Electron Microscopy Sciences, Ft.  
234 Washington, PA), and 1-µm thick sections were stained in 1% PPD for approximately 40 minutes.  
235 Stained sections were compared using a previously reported grading scale that is validated against  
236 axon counting (Howell et al., 2007; Howell et al., 2012). All cohorts included balanced numbers of male  
237 and female mice. We analyzed approximately 30 nerves for each strain and genotype, except for strain  
238 129 WT and D2-G mutant groups where we graded 15 and 17 nerves per group respectively. Groups  
239 were compared pairwise by Fisher's exact test.

#### 240 **Gene mapping and QTL analysis**

241 To identify loci controlling strain differences in phenotype onset and severity, *Lmx1b*<sup>+/+</sup> males of the  
242 glaucoma-susceptible B6 background were crossed to glaucoma-resistant 129.*Lmx1b*<sup>V265D/+</sup> female  
243 mice. 129B6F1 *Lmx1b*<sup>V265D/+</sup> mice were screened for anterior eye phenotypes by slit-lamp between 1-6  
244 months. 129B6F1 mice were resistant to *Lmx1b*'s effects, indicating that a dominant 129 locus(i)  
245 contributes to phenotypic resistance. To characterize this locus(i), we backcrossed 129B6F1  
246 *Lmx1b*<sup>V265D/+</sup> mice of both sexes to the B6 background to create an N2 recombinant mapping cohort. A  
247 total of 107 N2 *Lmx1b*<sup>V265D/+</sup> progeny of both sexes were aged and screened by slit-lamp and IOP  
248 measurement between 1-3 months and 4-5 months. We used slit-lamp data to map the genomic loci  
249 contributing to resistance. Based on slit-lamp data, each mapping mouse was binned into one of three  
250 categories; *bilateral susceptible* (B6-like), *bilateral resistant* (129-like), or *unilateral*. Mice were  
251 considered *bilateral susceptible* if one or more of the following phenotypes was at least moderate or  
252 severe in each eye; anterior chamber depth, pupil open, corneal haze, corneal opacity. If neither eye  
253 had any moderate or severe ocular phenotypes, mice were considered *bilateral resistant*. Due to  
254 variable expressivity, several mice had unilateral phenotypes affecting only the left or right eye in a  
255 random fashion. Genotyping was performed using 138 regularly spaced genome-wide single nucleotide  
256 polymorphic markers that differentiate the B6 and 129 genomes (SNPs, KBioscience, UK). We

performed a genome-wide one-dimensional quantitative trait locus (QTL) scan to identify the chromosomal loci modulating *Lmx1b* phenotypes. r/QTL version 1.14-2 was used for QTL analysis (Broman et al., 2003). The final QTL analysis uses mouse sex as an additive covariate and calculates genotype probability between SNP markers. QTL intervals were based on a 1.5 LOD drop from the maximum LOD peak on the chromosome. Because the first marker we genotyped on Chr 18 was at 5 Mb, we did not examine recombinants between 0-5 Mb. All genomic coordinates were calculated using GRCm38 (mm10) assembly.

## **Congenic strain generation and phenotyping**

The implicated Chr 18 modifier locus from strain 129 was backcrossed onto the B6 strain. This locus was selected using the slit-lamp based, phenotype severity data for 4-5 months old mice. At each generation of backcrossing, we used 5 markers to ensure transfer of the Chr 18 interval and flanking sequences (D18MIT19, D18MIT88, D18MIT123, D18MIT185, and D18Jmp6) to strain B6. After 10 or more generations, mice heterozygous (B6/129) at each of these Chr18 markers were crossed to B6.*Lmx1b*<sup>V265D/+</sup> mice to generate our experimental cohort and all experimental mice heterozygous for the modifier region were confirmed to have strain 129 alleles throughout the 69.5 Mb region. Mice were assessed by slit-lamp at 1-6 months of age and binned using the same *bilateral susceptible*, *bilateral resistant*, and *unilateral* groupings as for the N2 mapping mice. All groups contained balanced numbers of males and females and were compared by Fisher's exact test.

## **Results**

### **Strain 129 background is most resistant while B6 background is most susceptible**

Strain background had a profound effect on the ocular phenotypes in *Lmx1b*<sup>V265D/+</sup> mice (Fig. 1). Rare abnormal phenotypes were detected in some WT mice. This is due to the previously documented susceptibility of B6 mice to developmental abnormalities including anterior segment dysgenesis and anophthalmia (Chase, 1942; Gould and John, 2002; Smith et al., 1994). The frequency of these abnormalities varies based on factors such as environmental stress, and alcohol exposure (Cook et al., 1987; Sulik et al., 1981; Webster et al., 1983). Ocular disease phenotypes in *Lmx1b*<sup>V265D/+</sup> mutants included deepened anterior chambers, malformed and eccentric pupils, iridocorneal strands (strands of iris focally fused to cornea), corneal haze, corneal vascularization, corneal scleralization, and corneal ulceration (Fig. 1). We compared group differences in the frequency and severity of ocular phenotypes using Fisher's exact test. Of all examined strain backgrounds, 129.*Lmx1b*<sup>V265D/+</sup> mice were most

287 resistant to developing these abnormal ocular phenotypes (Fig. 1). When present in strain 129 mutants,  
288 phenotypes were generally mild (Figs 1,2). Overall, B6 mutants had the most developmentally severe  
289 phenotypic abnormalities of all backgrounds. Compared to D2-G mutants, B6 mutants develop more  
290 severe anterior chamber deepening at young ages (3-5 months) and more severe corneal haze at all  
291 ages (all  $P < 0.01$ , Fig. 2). C3H and B6 mutants were similar in phenotype severity across ages, except  
292 for corneal haze, which was significantly more severe in B6 mutants at young and intermediate ages (6-  
293 8 months;  $P < 0.01$ , Fig. 2). Therefore, overall B6.*Lmx1b*<sup>V265D/+</sup> are the most susceptible, C3H and D2-G  
294 backgrounds are intermediate, while strain 129 is the most resistant.

295

296 To test if the phenotypic differences are impacted by strain-dependent functional changes in the WT  
297 *Lmx1b* locus, we examined the *Lmx1b* locus of all four inbred strains using sequence data available  
298 from the Sanger Mouse Genomes Project (Keane et al., 2011). As 129/Sj and C3A/BLiA-*Pde6b*<sup>+</sup>/J were  
299 not available in the database, we used three closely related substrains of 129 (129P2/OlaHsd,  
300 129S1/SvlmJ, and 129S5SvEvBrd) and the closely related C3H/HeJ substrain respectively as proxies  
301 for the strain 129 and C3H genotypes. Compared to the B6 reference genome, neither the 129 nor C3H  
302 substrains have any coding regions or intergenic variants in conserved regions that would affect  
303 function. In contrast, the D2 background contains 3' UTR variants, synonymous coding variants, and a  
304 predicted splice region variant (rs27178126) 8bp from the splice donor site in intron 3. However,  
305 transcriptomic data from D2-G background limbal tissue showed no splicing abnormalities of any  
306 *Lmx1b* exons (data not shown). Given this, and the facts that 1) WT D2-G mice lack haploinsufficient  
307 *Lmx1b* phenotypes and 2) *Lmx1b*<sup>V265D/+</sup> D2-G mice are phenotypically similar to heterozygotes on the  
308 others strains and lack lethal homozygous mutant phenotypes, we conclude that the splice-region  
309 change has no effect. Additionally, as our most susceptible and resistant strains have identical *Lmx1b*  
310 loci, there is no clear relationship between the strain-specific WT *Lmx1b* locus and phenotypic severity.  
311 Furthermore, there are no changes in endogenous *Lmx1b* expression levels in ocular anterior segment  
312 tissue between wild type mice of the susceptible (B6) and resistant (129) inbred strains (Fig. S1). This  
313 indicates that other genetic modifier(s) underlie the observed phenotypic differences between these  
314 strains.

### 315 **B6.*Lmx1b*<sup>V265D/+</sup> mice have the most severely affected drainage structures**

316 Structural abnormalities in the aqueous humor drainage structures, Schlemm's canal (SC) and  
317 trabecular meshwork (TM), can lead to glaucoma by impacting IOP. These structures are located within  
318 the iridocorneal angle that runs around the entire limbal circumference of the eye. To evaluate whether  
319 strain background impacted drainage structure abnormalities in *Lmx1b*<sup>V265D/+</sup> mice, we analyzed the



320 morphology of the iridocorneal angle of our most extreme strains B6 and 129. WT mice have open  
321 drainage angles and normal SC and TM morphology (Fig. 3A). We found a spectrum of abnormalities in  
322 *Lmx1b*<sup>V265D/+</sup> mice of both B6 and 129 backgrounds including malformed or absent SC and/or TM as  
323 well as iridocorneal angle adhesions. Such abnormalities are expected to result in physical obstructions  
324 to aqueous humor outflow (closed angle; Fig. 3A). The effect on outflow will depend on the extent of  
325 such abnormalities around the eye, but outflow measurements were not performed. The severity of  
326 abnormalities in mutant mice varies both between eyes and locally around the angle circumference  
327 within individual eyes (Fig. 3A). Importantly, angle abnormalities were more severe in B6 background  
328 mutants compared to those of the 129 background (Mann-Whitney U Test,  $P = 0.0023$ ; Fig. 3B).  
329 Despite open-angle regions, B6 mutant angles were closed to aqueous humor drainage around much  
330 of the ocular circumference. However, strain 129 mutant angles were largely open and typically had  
331 only mild abnormalities. Mild iridocorneal angle abnormalities have been reported in patients with  
332 *LMX1B* variants and POAG (Lichter et al., 1997; Vollrath et al., 1998)

333 **IOP distribution is abnormal in *Lmx1b*<sup>V265D/+</sup> mice of all backgrounds with B6 being most severe**  
334 **at young ages.**

335 We longitudinally examined IOP in WT and *Lmx1b*<sup>V265D/+</sup> eyes and found an overall change to the  
336 distribution of IOP values in *Lmx1b*<sup>V265D/+</sup> eyes compared to WT controls. Spreading of IOP in both  
337 directions can be caused by various factors including ciliary body atrophy/malformation and corneal  
338 damage, as is most common in the *Lmx1b* B6 mutants here. Across all strain backgrounds and ages,  
339 mutant eyes had both the highest and lowest IOP values (Fig. 4A-C). The variance of WT and mutant  
340 IOP distributions was significantly different at all examined ages in B6, C3H, and D2-G backgrounds  
341 (Levene's test, all  $P < 0.01$ ). We found significantly elevated IOP in C3H (6-9 months), D2-G (3-6 and  
342 6-9 months), and strain 129 (3-6 and 6-9 months) mutants compared to WT controls (Fig. 4A,B;  
343 Welch's  $t$ -test, all  $P < 0.01$ ). Although IOP was clearly high in some eyes, the spreading of values in  
344 both directions masked the ability to detect mean differences compared to WT controls for other mutant  
345 groups. At 3-6 months, B6 mutants have a larger average dispersion (absolute difference from WT  
346 mean, see Methods) than D2-G and strain 129 mutants (Welch's  $t$ -test, all  $P < 0.01$ ; Fig. 4D).  
347 Consistent with this, 10% of B6 mutant eyes had IOP >30mmHg at 3-6 months, a magnitude not found  
348 in age-matched WT or mutant eyes of any other background (Fig. S2). C3H mutants did not have IOP  
349 assessed during the 3-6 months age window but appeared similar to B6 in anterior chamber  
350 deepening, a reflection of raised IOP. Although IOP abnormalities were detected in strain 129 mutants  
351 at different ages, there was significantly less IOP dispersion in these mice at advanced ages (9-12  
352 months) compared to all other backgrounds (Welch's  $t$ -test, all  $P < 0.01$ ; Fig. 4F). Overall, our data

353 shows that *Lmx1b*<sup>V265D</sup> has a strong impact on IOP with the most extreme and earliest phenotypes on a  
354 B6 background.

355 **B6.*Lmx1b*<sup>V265D/+</sup> mice develop severe glaucoma but 129.*Lmx1b*<sup>V265D/+</sup> mice do not**

356 To assess the extent to which IOP elevation leads to glaucomatous neurodegeneration across genetic  
357 backgrounds, we histologically assessed retinas and optic nerves of *Lmx1b*<sup>V265D/+</sup> and WT mice.  
358 Because the majority of abnormally elevated IOP values are found at 3-6 and 6-9 months in  
359 B6.*Lmx1b*<sup>V265D/+</sup> mice, we examined their optic nerves between 10-12 months. Optic nerves of D2-G  
360 and 129 backgrounds were examined slightly later in life (12-14 months). Consistent with other ocular  
361 phenotypes, B6.*Lmx1b*<sup>V265D/+</sup> mice had the highest prevalence of severely degenerated optic nerves  
362 with nearly 80% of nerves having severe axon loss and damage and prominent gliosis (Fig. 5A,B).  
363 Importantly, mutants on the 129 background did not develop any detectable optic nerve degeneration  
364 (Fig. 5A), even at the oldest age examined. Mutants with optic nerve degeneration had characteristic  
365 hallmarks of glaucoma with retinal nerve fiber layer thinning (layer containing retinal ganglion cell  
366 axons) and optic nerve excavation/remodeling (Fig. 5C).

367 **The BALB background does not increase disease severity**

368 Mutation of the tyrosinase gene (*Tyr*) increases susceptibility to ocular drainage tissue defects in  
369 *Cyp1b1* and *Foxc1* mutants (Libby et al., 2003). To assess the effect of an additional genetic  
370 background and if *Lmx1b*-induced disease onset is earlier in a *Tyr* deficient background, we crossed  
371 the *Lmx1b*<sup>V265D/+</sup> allele to the albino BALB/cJ (BALB) strain background and analyzed 3 to 6 months old  
372 mice (Yokoyama et al., 1990). Compared to our most susceptible B6 background, BALB mutant mice  
373 are resistant to *Lmx1b*-induced anterior segment developmental phenotypes (Fig. S3, Table S1).  
374 Similar to strain 129 mutants, anterior segment phenotypes in BALB mutants were generally mild when  
375 present. BALB mutants did develop elevated IOP with their IOP distribution being similar to the other  
376 backgrounds (Fig. S3, Table S2). Therefore, *Tyr* genotype did not exacerbate disease severity in  
377 *Lmx1b* mutants on a BALB background.

378 **A locus on Chromosome 18 determines differential susceptibility to *Lmx1b*-associated**  
379 **phenotypes**

380 In order to identify genomic regions contributing to differential susceptibility between the B6 and 129  
381 genetic backgrounds, we performed a mapping cross. Specifically, F1 progeny were generated using  
382 males from the susceptible B6 background and *Lmx1b*<sup>V265D/+</sup> females from the more resistant 129

background. 129B6 *Lmx1b*<sup>V265D/+</sup> F1's phenocopied 129 mutants indicating 129-dominant loci confer disease resistance (data not shown). Thus, we backcrossed F1's to B6 to generate N2 mutant mapping progeny. Based on the severity of ocular phenotypes as assessed by slit-lamp at each examined age, N2 *Lmx1b*<sup>V265D/+</sup> mice were binned into a *bilateral susceptible* (B6-like), *bilateral resistant* (129-like), or *unilateral* categories. The unilateral category was used when only a single eye displayed severe abnormalities and reflects reduced susceptibility to *Lmx1b*<sup>V265D/+</sup>-induced phenotypes. All N2 mapping progeny were genotyped using single nucleotide polymorphic (SNP) marker analysis. Using this data, we performed a quantitative trait locus (QTL) scan in our N2 cohort against ocular phenotype severity. In 1 to 3 months old mice, we detected intervals on Chromosomes 1 (33-139 Mb, max LOD at 53.6 Mb) and 18 (5-71.7 Mb, max LOD at 30.9 Mb) that significantly associated with slit-lamp based phenotype severity using a genome-wide significance cutoff (Fig. 6A). At 4 to 5 months, however, only the interval on chromosome 18 (5-74.5 Mb, max LOD at 30.9 Mb) reached genome-wide significance using the slit-lamp based phenotype severity data (Fig. 6B). To test whether the Chr 18 locus is sufficient to generate resistance to disease phenotypes in *Lmx1b* mutants, we backcrossed the strain 129 Chr 18 interval onto the B6 background. B6.*Lmx1b*<sup>V265D/+</sup> mice that were heterozygous B6/129 throughout the Chr 18 interval were significantly more resistant to the *Lmx1b*-induced slit-lamp phenotypes than littermates that were homozygous B6 (Fisher's exact test,  $P=0.036$ ; Fig. 6C). This further supports the resistance locus and future experiments are required to refine it.

## Discussion

### Differing disease presentation between individuals

Recent GWAS studies indicate that *LMX1B* variants cause elevated IOP and glaucoma in the general human population, without evident anterior segment abnormalities, involvement of other organs/tissues, or NPS diagnosis (Choquet et al., 2018; Gao et al., 2018; Gharahkhani et al., 2018; Khawaja et al., 2018; MacGregor et al., 2018; Shiga et al., 2018). Similarly, *LMX1B* mutations cause organ specific kidney disease without extrarenal involvement (Boyer et al., 2013; Isojima et al., 2014). Several factors may contribute to differing disease presentations between individuals including the nature of the *LMX1B* variant, genetic modifiers, and environmental factors. Here, we clearly show that genetic background has a strong influence on disease presentation. This effect of genetic background allows a path to deciphering key pathogenic mechanisms through characterization of modifier genes. Additionally, this effect must be considered when interpreting experimental data. For example, previous studies report that mice heterozygous for a null allele of *Lmx1b* have normal eyes on both a C57BL/6J and a C57BL/6x129/Sv mixed background respectively (Cross et al., 2014; Pressman et al., 2000).

415 Haploinsufficiency is generally accepted to contribute to human disease, as heterozygous deletions  
416 including *LMX1B* are pathogenic (Bongers et al., 2008; McIntosh et al., 1998). Thus, it remains unclear  
417 if mice differ to humans in their sensitivity to haploinsufficiency-induced phenotypes or if null alleles will  
418 induce characteristic abnormalities when assessed on further genetic backgrounds.

419 The nature of the mutation in *Lmx1b* is important to consider. The pathogenic nature of *LMX1B*  
420 haploinsufficiency suggests reduced transcription factor dosage or activity causes disease. However,  
421 as demonstrated by the *Lmx1b*<sup>V265D</sup> allele, different mechanisms apart from haploinsufficiency can  
422 contribute to glaucoma such as dominant negative effects (Cross et al., 2014). The location of the point  
423 mutation within human *LMX1B* correlates with disease severity in the kidney (Bongers et al., 2005).  
424 Additional functional characterization of *LMX1B* mutations is required to better understand how the  
425 nature of the *LMX1B* variant affects disease onset and severity. Recently, a dominant stop codon  
426 mutation (*Lmx1b*<sup>Q105X</sup>, reported as *Lmx1b*<sup>Q82X</sup>) was shown to cause IOP elevation and glaucoma  
427 without anterior segment developmental abnormalities (by slit-lamp) on the D2-G background (Choquet  
428 et al., 2018). This contrasts to the *Lmx1b*<sup>V265D</sup> allele, which induces obvious anterior segment  
429 abnormalities on the same D2-G genetic background (Figs 1-3). Together, these data strengthen the  
430 suggestion that the nature of individual *LMX1B* alleles affects the range and severity of disease  
431 outcomes in human patients (Bongers et al., 2005; McIntosh et al., 1998). Characterizing different  
432 mutant alleles on genetically diverse backgrounds will be important in determining disease mechanisms  
433 and discovering genetic modifiers, with the goal of improving risk assessment and developing  
434 therapeutics (Jeanne and Gould, 2017).

### 435 **Mechanisms of IOP elevation**

436 *LMX1B* variants are known to disrupt drainage structure development and cause developmental and  
437 juvenile onset glaucoma (Lichter et al., 1997; Liu and Johnson, 2010; Pressman et al., 2000;  
438 Sawamura et al., 2014). These developmental changes lead to drainage structure abnormalities and  
439 IOP elevation. Our data clearly show that all *Lmx1b*<sup>V265D/+</sup> eyes have structural abnormalities of their  
440 iridocorneal angle. B6 mutants had the greatest severity of angle abnormalities and the most severely  
441 dysregulated IOPs at younger ages. This suggests that developmental drainage structure abnormalities  
442 are important in IOP elevation in these mice. Future work is required to determine how these structural  
443 deficits impact resistance to AqH drainage. 129.*Lmx1b*<sup>V265D/+</sup> mice have milder iridocorneal angle  
444 structural abnormalities with the vast majority of the angle being open, but they still develop elevated  
445 IOP. Mild iridocorneal angle defects are found in POAG patients with NPS, which is caused by *LMX1B*

446 variants (Lichter et al., 1997; Vollrath et al., 1998). Thus, strain 129 mutants are a valuable resource to  
447 model IOP elevation in POAG due to *LMX1B* variants.

448 Although structural developmental changes cause early-onset elevated IOP in some mutants, IOP  
449 becomes high at older ages in other *Lmx1b* mutants. As mutant eyes have less functional drainage  
450 tissue to begin with, the remaining functional tissue may be more susceptible to damage with age,  
451 leading to later-onset IOP elevation. It is possible that mechanisms unrelated to structure or normal  
452 drainage-function are involved in *Lmx1b*-phenotypes during development or adult life (Gould et al.,  
453 2004). Mutants may have abnormal metabolism or suboptimal defense mechanisms against ongoing  
454 stressors (e.g. oxidative stress) leading to tissue demise and IOP elevation over time. In agreement  
455 with this, the majority of patients with *LMX1B* variants have primary open angle glaucoma (Sweeney et  
456 al., 2003). These patients develop IOP elevation at older ages and have an open drainage angle with  
457 no obvious structural abnormalities. The mechanisms by which *LMX1B* variants impact the function of  
458 drainage tissue in POAG are likely complex and require additional characterization. In the current  
459 study, we did not explore whether the *Lmx1b*<sup>V265D</sup> mutation directly impacts retinal development or  
460 retinal ganglion cell degeneration. Studies in zebrafish show that *Lmx1b* orthologues *Lmx1b.1* and  
461 *Lmx1b.2* are necessary for normal retinal patterning including ventral optic cup morphogenesis  
462 (McMahon et al., 2009). Arguing against a key effect on retinal development in *Lmx1b*<sup>V265D</sup> mice,  
463 previous work found no retinal or optic nerve abnormalities in 90% of mice at 8 months of age (Cross et  
464 al., 2014). By 10-11 months, however, >60% of the nerves had developed severe degeneration,  
465 indicating that glaucomatous nerve damage is age related in these *Lmx1b* mutants (Cross et al., 2014).  
466 In the current study, *Lmx1b* mutants on strain backgrounds with the most severe incidence of anterior  
467 chamber deepening (a symptom of IOP elevation) and the most abnormal IOP distributions have the  
468 highest incidence of neurodegeneration. Together, these data suggest that IOP elevation is a primary  
469 factor driving neurodegeneration. Still, it remains possible that the *Lmx1b*<sup>V265D</sup> mutation sensitizes  
470 retinal cells to degeneration and further experiments are needed to test this.

471 In addition to IOP elevation, abnormally low IOP was found in *Lmx1b*<sup>V265D/+</sup> mice on each strain  
472 background at various ages. Abnormally low IOP is observed in other mouse models with abnormal  
473 anterior segment development (Chang et al., 2001). One contributing factor could be dysgenesis of the  
474 ciliary body, which produces AqH (Chang et al., 2001). *Lmx1b* is expressed in the developing ciliary  
475 body (Pressman et al., 2000), and the *Lmx1b*<sup>V265D</sup> allele could potentially cause dysfunction of AqH  
476 production. Additionally, the *Lmx1b*<sup>V265D</sup> allele induces severe corneal phenotypes involving extensive  
477 stretching, ulceration, and perforation, that contribute to lower than normal IOP. B6.*Lmx1b*<sup>V265D/+</sup> mice

478 have the highest incidence of abnormally low IOP values and the most severely affected corneas,  
479 consistent with a role of corneal phenotypes in lowering IOP.

## 480 **Identifying the genetic modifiers**

481 The genetic loci that modify glaucoma susceptibility in individuals with *LMX1B* variants are not known.  
482 The interactions between these loci are likely complex. We discovered QTL on Chromosomes 1 and 18  
483 that predispose *Lmx1b*<sup>V265D/+</sup> mice to severe ocular abnormalities. Future work is required to  
484 characterize specific modifiers, to understand disease risk of individuals with *LMX1B* mutations, and  
485 provide molecular targets for therapies to treat IOP elevation and glaucoma. Future studies are also  
486 required to directly test QTL impacting IOP, outflow facility, and axon counts in *Lmx1b* mutant mice.  
487 Although the Chr 1 locus may be important, its effect was only evident at the youngest analyzed age.  
488 We chose to conduct follow up experiments on the Chr 18 locus because it had an effect at both  
489 assessed ages. As the 69.5 megabase interval on Chr 18 contains approximately 442 protein-coding  
490 genes, we are currently unable to nominate specific candidates responsible for strain-specific  
491 differences in susceptibility, limiting our ability to pursue the underlying mechanisms. Ongoing work is  
492 aimed at prioritizing positional candidates. Based on published literature, 5 of the 442 genes are  
493 associated with human glaucoma, elevating them as candidate genes within the interval. However,  
494 none of the 5 corresponding mouse loci have SNPs between B6 and 129 mice that are predicted to  
495 impact transcript abundance or protein function [Table S3; (Keane et al., 2011)]. Regarding genetic  
496 differences between strains B6 and 129, an interval around the Zinc finger E-box-binding homeobox 1  
497 (*ZEB1*) locus harbors several variants, including predicted functional variants in *ZEB1* (Keane et al.,  
498 2011). Interestingly, *ZEB1* variants cause Fuch's corneal endothelial dystrophy (FCED) (Gupta et al.,  
499 2015). In FCED, the corneal endothelial structure is disrupted causing corneal haze. Corneal haze  
500 differs significantly between B6 and strain 129 *Lmx1b* mutant mice at each examined age. Furthermore,  
501 *Zeb1* null mouse embryos have ocular developmental defects similar to *Lmx1b* mutants including  
502 iridocorneal adhesions (Liu et al., 2008). However, no links are yet established between *ZEB1* and IOP  
503 elevation or *LMX1B*. Therefore, although *ZEB1* is an intriguing candidate, the modifier interval requires  
504 further refinement before a specific locus can be identified. In conclusion, this study lays a strong  
505 foundation for better understanding mechanisms by which *LMX1B* contributes to glaucoma and for  
506 characterizing new therapeutic targets.

## 507 **Acknowledgements**

508 The Authors would like to thank the Histology Services and Computational Services at The Jackson  
509 Laboratory, animal care staff at The Jackson laboratory and Columbia University, and Amy Bell for  
510 intraocular pressure measurements.

511 **Funding**

512 EY011721 (SWMJ), Barbara and Joseph Cohen Foundation Precision Medicine Initiative at Columbia  
513 University (SWMJ), unrestricted departmental funds from research to prevent blindness and core grant  
514 P30EY019007 (SWMJ). UK Medical Research Council to MRC Human Genetics Unit, programme  
515 MC\_PC\_U12756112 (IJJ), EY027004 (KSN), EY022891 (KSN), G2019360 (KSN), EY028175 (KK),  
516 T32HD007065 (NGT). Simon John is an investigator of HHMI.

517 **Conflict of interest statement**

518 The authors declare no competing or financial interests.

**Barbara and Joseph Foundation separate**

**Precision**

519 **Figures/Tables:**

520 **Table 1.** Severity definitions for abnormalities in *Lmx1b*<sup>V265D/+</sup> mice

Phenotype Evaluated	Severity	Observation
Anterior chamber deepening	Normal	AC visible by slit-lamp with normal, just-detectable gap between cornea and iris
	Mild	AC visible by slit-lamp side view as clear but thin gap between cornea and iris
	Moderate	AC visible by slit-lamp side view with a prominent gap between cornea and iris
	Severe	Clearly detectable buphthalmous by naked eye
Pupil abnormalities	Normal	Pupil is centered in iris, circular, and 0.3mm (+/- 0.1mm) diameter
	Mild	Pupil is eccentric or mis-shaped, not centered in iris, and/or is up to 2X wider than normal diameter
	Moderate	As above, but more severely misshaped and/or up to 4X normal diameter
	Severe	As above, but more severely misshapen and greater than 4X normal diameter
Corneal haze	Normal	Cornea completely transparent
	Mild	Transparency of cornea is slightly disrupted (can clearly visualize iris and lens)
	Moderate	Transparency of cornea is significantly impacted (difficult to visualize iris and lens)
	Severe	Transparency of cornea is completely lost (cannot see structures through cornea)
Corneal vascularization, scarring, and ulceration	Normal	No vascularization, scarring, or ulceration present
	Mild	Small focal point in cornea with vascularization, scarring, and/or ulcer
	Moderate	Obvious vascularization, scarring, and/or ulcer covering up to 50% of cornea
	Severe	Vascularization, scarring, and/or ulcer covering more than 50% of cornea

521 AC, anterior chamber



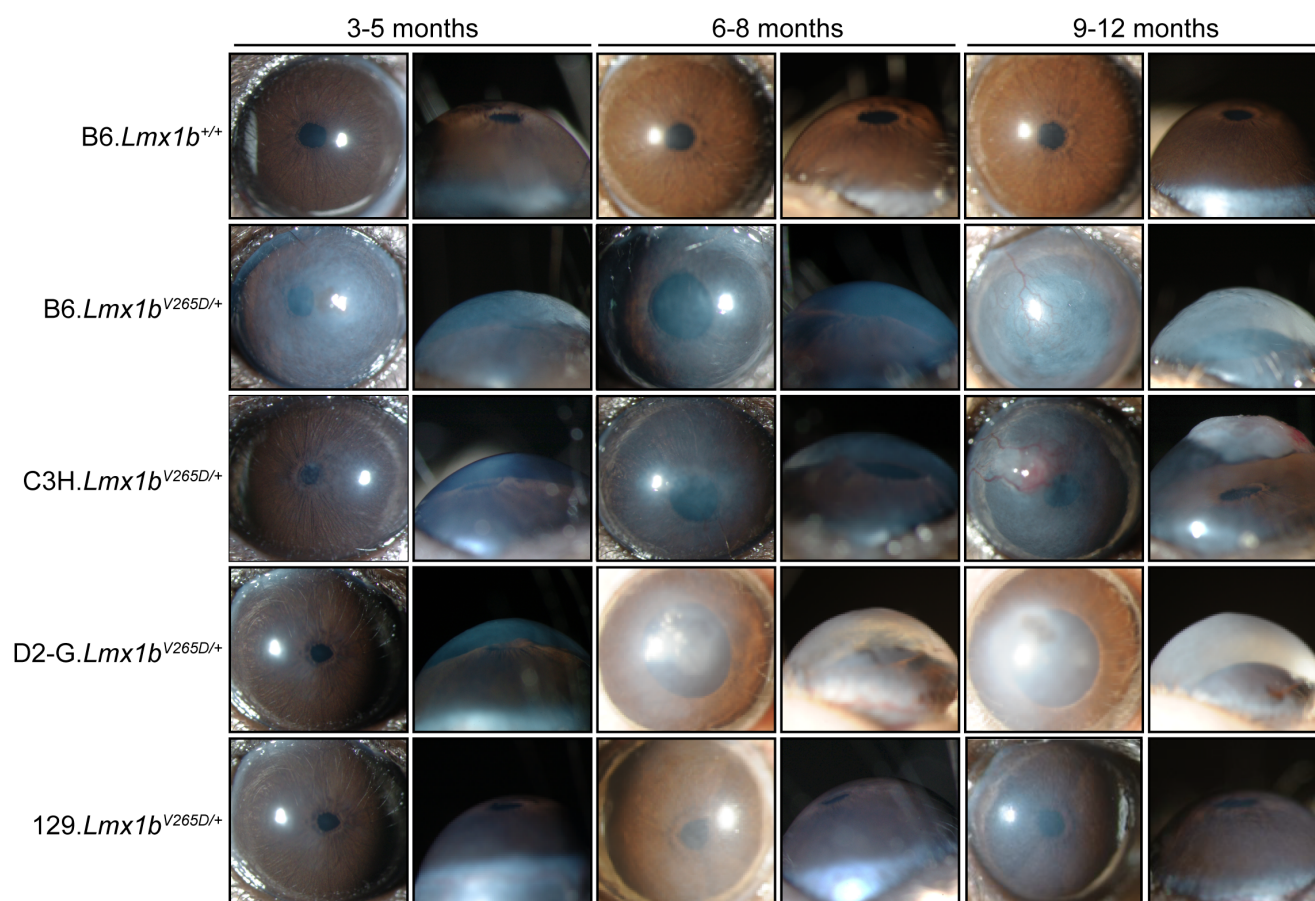


**Figure 1: Strain background alters phenotypes in *Lmx1b*<sup>V265D/+</sup> mice.** Representative front and side-view, slit-lamp images for mice of the indicated ages and genotypes. The frequencies of specific disease features are shown in Figure 2. WT mice of all backgrounds were similar and so only B6 WT mice are shown. B6.*Lmx1b*<sup>V265D/+</sup> mutant mice have the most severe overall phenotypes including malformed eccentric pupils, extensive corneal haze and greatly deepened anterior chambers at 3 months of age. With age, the severity of B6 phenotypes increases, with development of corneal scarring, vascularization, and ulcers. C3H mutants are generally similar to B6 but are more resistant to developmental corneal phenotypes at younger ages. D2-G mutants are generally similar to C3H, but more resistant to LMX1B-induced corneal phenotypes at all ages (see Figure 2). The 129 strain background is the most resistant, with mutants typically displaying only mild pupillary abnormalities and corneal haze.

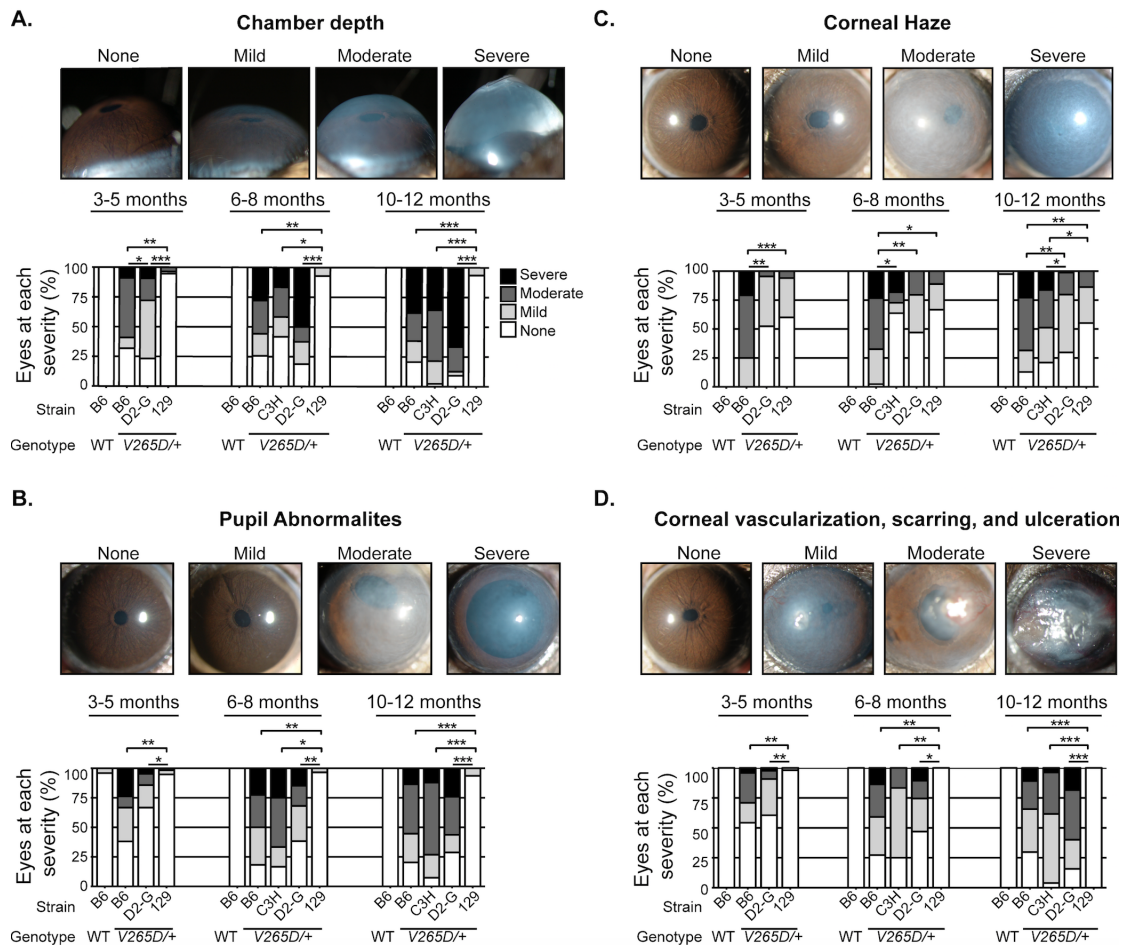
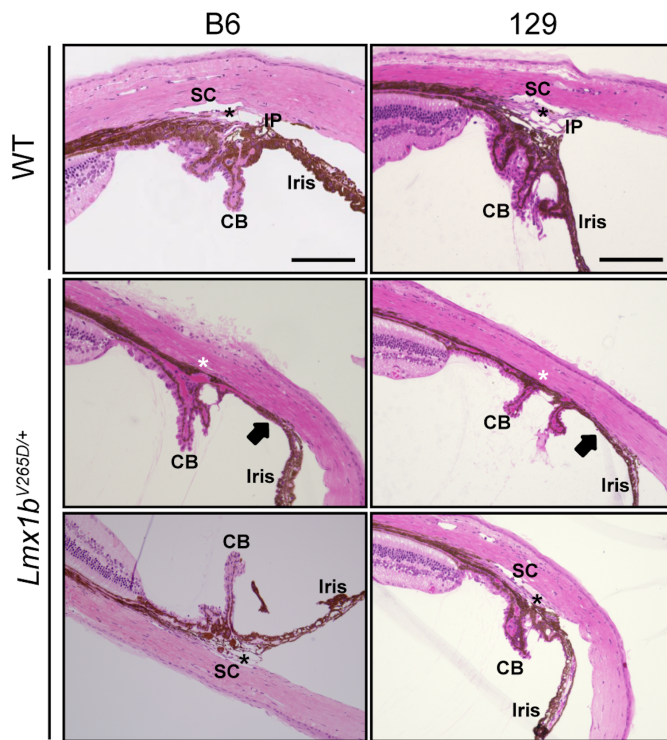


**Figure 2: B6 background is most susceptible, while strain 129 is most resistant. (A)** At 3-5 months, B6 mice have the most severe anterior chamber deepening (ACD), even compared to D2-G mutants ( $P = 0.0034$ ). Strain 129 mutants rarely develop abnormal ACD at any age. Anterior chamber deepening (ACD) is a symptom of IOP elevation. (B-D) The same was true for corneal haze, pupillary and corneal abnormalities. \*  $P < 0.01$ ; \*\*  $P < 1.0E-05$ ; \*\*\*  $P < 1.0E-10$  (see supplementary table 1 for exact  $P$  values).

# A. Iridocorneal Angle Sections (3 months)



# B. Angle Score (3 months)

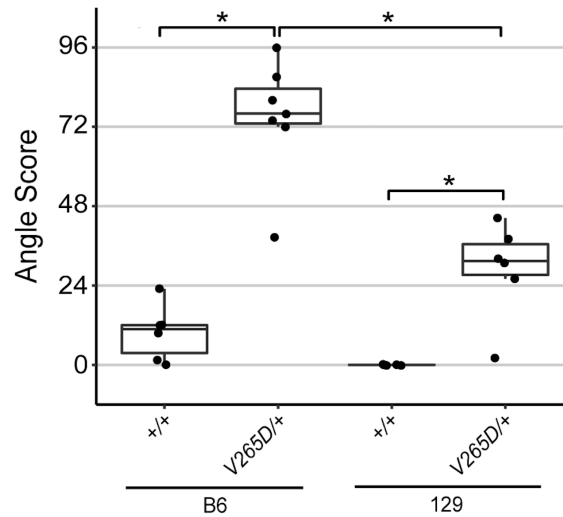
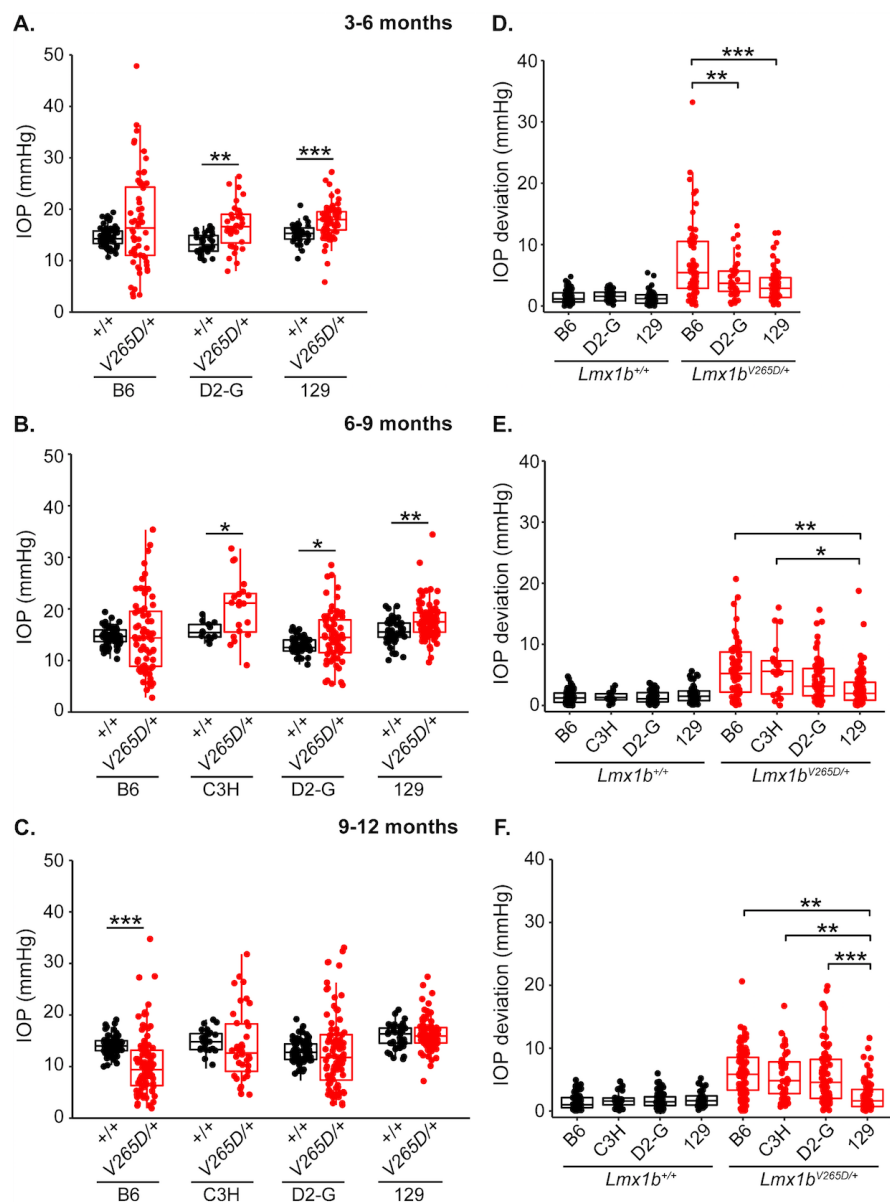


## Figure 3: 129.*Lmx1b*<sup>V265D/+</sup> mutants are resistant to angle abnormalities compared to B6. (A)

Representative images of the iridocorneal angle region (H&E stained sagittal sections) in 3 months old mice. WT mice of both B6 and 129 backgrounds have normal open-angle morphology. Narrow iris processes (IP), are known to occur intermittently around the angle of WT mice without obstructing aqueous humor drainage. SC: Schlemm's canal, black asterisk: trabecular meshwork, CB: ciliary body. In mutant eyes, abnormalities, including severe iridocorneal adhesions (arrows) as well as absent (white asterisk) or hypomorphic SC and TM, are locally present within individual eyes (middle panels) with different locations within the same eyes having open-angles of normal morphology (bottom panels). Scale bar = 200µm. (B) B6 mutant have high angle scores (Methods), indicating largely closed or malformed angles. Strain 129 mutants have less severely affected, largely open-angles. Higher angle scores indicate a more severely and more extensively affected angle around its circumference. A score of 96 represents a severely abnormal angle at all locations while an angle with a score of 0 being is completely normal and open at all locations. The strain 129 median grade of 31 indicates that their angles were open at most locations around the eye. It is established that a small incidence of developmental abnormalities occurs in B6 WT mice (see main text). Boxplots show interquartile range and median line. Mann-Whitney U test; \* =  $P < 0.01$  (129 vs B6 mutants,  $P = 0.0023$ ; 129 WT vs mutant

558  $P = 0.0055$ ; B6 WT vs mutant,  $P = 0.0033$ ). We examined 5 eyes from the strain 129 WT group, 6 eyes  
559 from the strain 129 mutant and B6 WT groups, and 7 eyes from the B6 mutant group.



560

561 **Figure 4: IOP in *Lmx1b* mutants (A-C)** Boxplots of IOP (interquartile range and median line) clearly  
 562 indicate spreading of IOP in mutants of all strain backgrounds with clear IOP elevation in some  
 563 mutants. **(A-B)** *Lmx1b*<sup>V265D/+</sup> mutants of D2-G and strain 129 backgrounds have significantly elevated  
 564 IOP compared to respective WT controls at 3-6 mo and 6-9 mo. C3H mutants have elevated IOP at 6-9  
 565 months compared to WT controls ( $P = 0.0032$ ). Although IOP was not measured, anterior chamber  
 566 deepening suggests IOP is elevated in many C3H mutants prior to 6 months age (Figure 1) **(C)** Due to  
 567 an increase in abnormally low IOP values, B6.*Lmx1b*<sup>V265D/+</sup> mice have a significantly lower IOP average  
 568 than WT controls at 9-11 months old ( $P = 8.2E-7$ ). **(D-F)** Boxplots of IOP deviation (absolute value of

569 difference to respective WT mean value, Methods) At all ages, WT groups had minimal IOP deviation,  
570 with no values deviating more than 7mmHg. **(D)** At 3-5 months, B6 mutants have a significantly greater  
571 IOP deviation compared to those of D2-G ( $P = 0.0068$ ) and strain 129 ( $P = 4.5E-05$ ) backgrounds. **(E-**  
572 **F)** Strain 129 mutants have significantly less IOP deviation compared to B6 and C3H mutants at 6-9  
573 months and to all other backgrounds 9-12 months. \*  $P < 0.01$ , \*\*  $P < 0.001$ , \*\*\*  $P < 0.0001$  (see  
574 supplementary table 2 for exact  $P$  values).



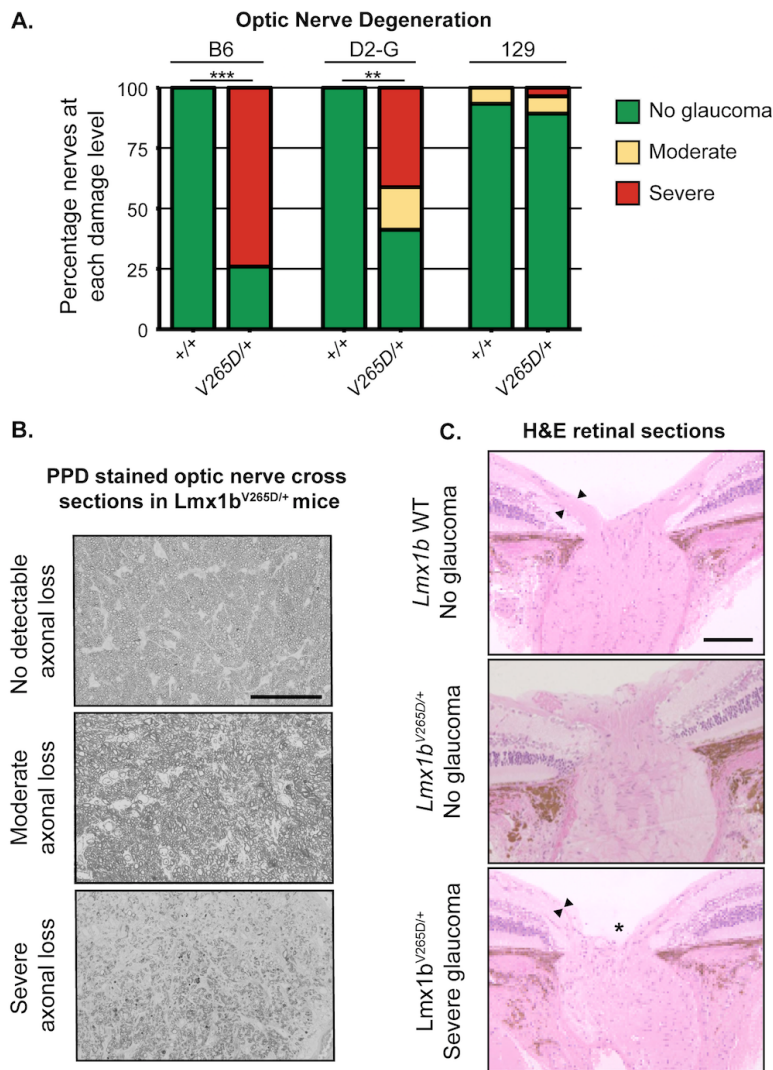


**Figure 5: B6.*Lmx1b*<sup>V265D/+</sup> mice develop glaucomatous neurodegeneration while 129.*Lmx1b*<sup>V265D/+</sup> mice do not. (A)** Frequency histogram of degree of optic nerve damage evident in PPD stained cross sections (Methods) \*\*  $P < 1.0E-05$ , \*\*\*  $P < 1.0E-10$ . **(B)** Representative images of PPD-stained optic nerve cross sections from *Lmx1b*<sup>V265D/+</sup> mice. (Top) Healthy nerves at 10 months old had no detectable axonal damage. These axons had a clear axoplasm and darkly stained myelin sheaths. (Middle) Moderate optic nerve degeneration with some axon loss and early gliosis. (Bottom) Severe damage and extreme axon loss with extensive glial scarring. Scale bar = 50µm **(C)** H&E stained optic nerve heads with flanking retina. WT eyes have normal nerve heads with a thick nerve fiber layer (arrowheads) as do unaffected mutants. Severely affected mutants have pronounced optic nerve excavation (asterisk) with loss of the nerve fiber layer (arrowheads), Scale bar = 200µm.

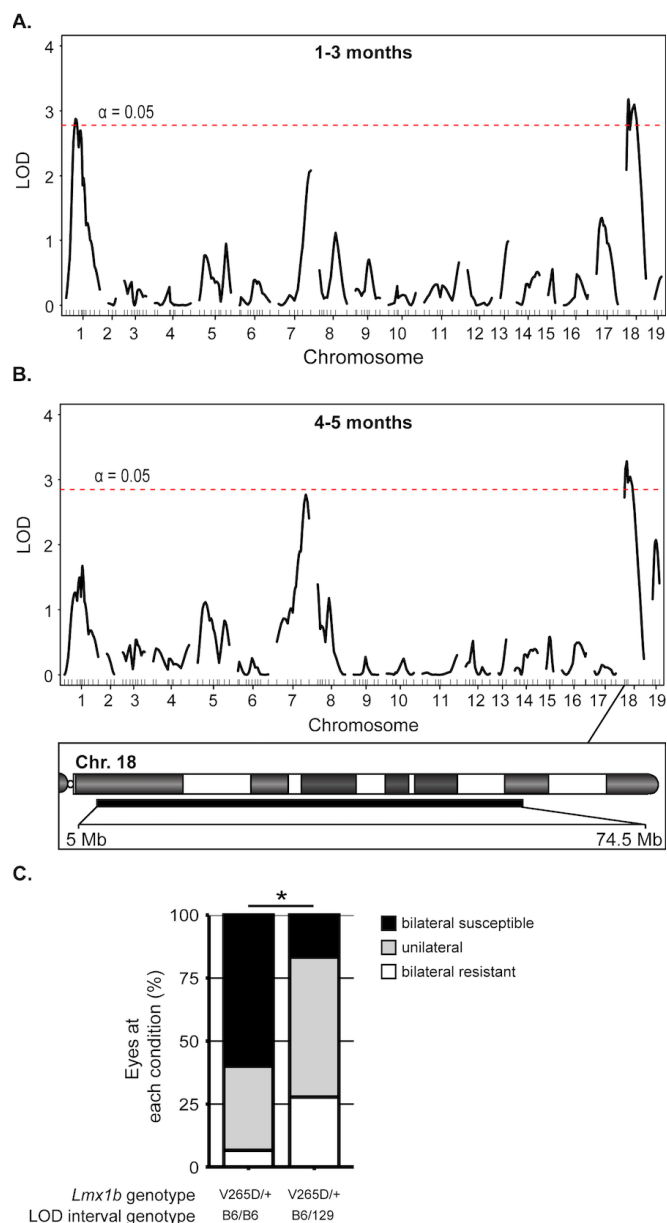


**Figure 6: Modifier loci.** Based on slit-lamp data, individual N2 mice were binned into one of three categories; *bilateral susceptible* (B6-like), *bilateral resistant* (129-like), or *unilateral*. Using this data, a genome-wide one-dimensional quantitative trait locus (QTL) scan was performed. **(A)** At 1-3 months, intervals on both Chr 1 (33-139 Mb, max LOD at 53.6 Mb) and Chr 18 (5-71.7 Mb, max LOD at 30.9 Mb) reached genome wide significance (5% significance threshold, genome-wide corrected, red dotted line). **(B)** At 4-5 months, an interval on Chr18 (5-74.5 Mb, max LOD at 30.9 Mb) with the same max LOD as 1-3 months was identified at genome wide significance. **(C)** Testing of the modifier locus by comparing *Lmx1b*<sup>V265D/+</sup> mutant mice that are either homozygous (B6/B6) or heterozygous (B6/129) for



the Chr 18 intervals. Having a strain 129 genotype throughout the modifier interval significantly increased resistance to severe ocular phenotypes compared to B6 homozygous littermates (Fisher's exact test,  $P = 0.036$ ). *Lmx1b* WT mice that are B6/129 heterozygous for the Chr 18 interval did not develop anterior eye phenotypes (data not shown). We examined 15 (Chr 18 B6/B6) and 18 (Chr 18 B6/129) mice.

## References

- Beals, R. K. and Eckhardt, A. L. (1969). Hereditary onycho-osteodysplasia (Nail-Patella syndrome). A report of nine kindreds. *J Bone Joint Surg Am* **51**, 505-16.
- Bennett, W. M., Musgrave, J. E., Campbell, R. A., Elliot, D., Cox, R., Brooks, R. E., Lovrien, E. W., Beals, R. K. and Porter, G. A. (1973). The nephropathy of the nail-patella syndrome. Clinicopathologic analysis of 11 kindred. *Am J Med* **54**, 304-19.
- Bongers, E. M., de Wijs, I. J., Marcelis, C., Hoefsloot, L. H. and Knoers, N. V. (2008). Identification of entire LMX1B gene deletions in nail patella syndrome: evidence for haploinsufficiency as the main pathogenic mechanism underlying dominant inheritance in man. *Eur J Hum Genet* **16**, 1240-4.
- Bongers, E. M., Huysmans, F. T., Levtschenko, E., de Rooy, J. W., Blickman, J. G., Admiraal, R. J., Huygen, P. L., Cruysberg, J. R., Toolens, P. A., Prins, J. B. et al. (2005). Genotype-phenotype studies in nail-patella syndrome show that LMX1B mutation location is involved in the risk of developing nephropathy. *Eur J Hum Genet* **13**, 935-46.
- Bonnemaijer, P. W. M., Iglesias, A. I., Nadkarni, G. N., Sanyiwa, A. J., Hassan, H. G., Cook, C., Group, G. S., Simcoe, M., Taylor, K. D., Schurmann, C. et al. (2018). Genome-wide association study of primary open-angle glaucoma in continental and admixed African populations. *Hum Genet* **137**, 847-862.
- Boyer, O., Woerner, S., Yang, F., Oakeley, E. J., Linghu, B., Gribouval, O., Tete, M. J., Duca, J. S., Klickstein, L., Damask, A. J. et al. (2013). LMX1B mutations cause hereditary FSGS without extrarenal involvement. *J Am Soc Nephrol* **24**, 1216-22.
- Broman, K. W., Wu, H., Sen, S. and Churchill, G. A. (2003). R/qt1: QTL mapping in experimental crosses. *Bioinformatics* **19**, 889-90.
- Chang, B., Smith, R. S., Peters, M., Savinova, O. V., Hawes, N. L., Zabaleta, A., Nusinowitz, S., Martin, J. E., Davisson, M. L., Cepko, C. L. et al. (2001). Haploinsufficient *Bmp4* ocular phenotypes include anterior segment dysgenesis with elevated intraocular pressure. *BMC Genet* **2**, 18.
- Chase, H. B. (1942). Studies on an Anophthalmic Strain of Mice. III. Results of Crosses with Other Strains. *Genetics* **27**, 339-48.
- Chen, H., Lun, Y., Ovchinnikov, D., Kokubo, H., Oberg, K. C., Pepicelli, C. V., Gan, L., Lee, B. and Johnson, R. L. (1998). Limb and kidney defects in *Lmx1b* mutant mice suggest an involvement of LMX1B in human nail patella syndrome. *Nat Genet* **19**, 51-5.
- Choquet, H., Paylakhi, S., Kneeland, S. C., Thai, K. K., Hoffmann, T. J., Yin, J., Kvale, M. N., Banda, Y., Tolman, N. G., Williams, P. A. et al. (2018). A multiethnic genome-wide association study of primary open-angle glaucoma identifies novel risk loci. *Nat Commun* **9**, 2278.
- Choquet, H., Thai, K. K., Yin, J., Hoffmann, T. J., Kvale, M. N., Banda, Y., Schaefer, C., Risch, N., Nair, K. S., Melles, R. et al. (2017). A large multi-ethnic genome-wide association study identifies novel genetic loci for intraocular pressure. *Nat Commun* **8**, 2108.
- Choquet, H., Wiggs, J. L. and Khawaja, A. P. (2020). Clinical implications of recent advances in primary open-angle glaucoma genetics. *Eye (Lond)* **34**, 29-39.

637 **Cook, C. S., Nowotny, A. Z. and Sulik, K. K.** (1987). Fetal alcohol syndrome. Eye malformations in a  
638 mouse model. *Arch Ophthalmol* **105**, 1576-81.

639 **Craig, J. E., Han, X., Qassim, A., Hassall, M., Cooke Bailey, J. N., Kinzy, T. G., Khawaja, A. P., An, J.,**  
640 **Marshall, H., Gharahkhani, P. et al.** (2020). Multitrait analysis of glaucoma identifies new risk loci and enables  
641 polygenic prediction of disease susceptibility and progression. *Nat Genet* **52**, 160-166.

642 **Cross, S. H., Macalinao, D. G., McKie, L., Rose, L., Kearney, A. L., Rainger, J., Thaung, C., Keighren, M.,**  
643 **Jadeja, S., West, K. et al.** (2014). A dominant-negative mutation of mouse Lmx1b causes glaucoma and is semi-  
644 lethal via LDB1-mediated dimerization [corrected]. *PLoS Genet* **10**, e1004359.

645 **Dreyer, S. D., Zhou, G., Baldini, A., Winterpacht, A., Zabel, B., Cole, W., Johnson, R. L. and Lee, B.**  
646 (1998). Mutations in LMX1B cause abnormal skeletal patterning and renal dysplasia in nail patella syndrome. *Nat*  
647 *Genet* **19**, 47-50.

648 **Farley, F. A., Lichter, P. R., Downs, C. A., McIntosh, I., Vollrath, D. and Richards, J. E.** (1999). An  
649 orthopaedic scoring system for nail-patella syndrome and application to a kindred with variable expressivity and  
650 glaucoma. *J Pediatr Orthop* **19**, 624-31.

651 **Fautsch, M. P. and Johnson, D. H.** (2006). Aqueous humor outflow: what do we know? Where will it  
652 lead us? *Invest Ophthalmol Vis Sci* **47**, 4181-7.

653 **Gao, X. R., Huang, H., Nannini, D. R., Fan, F. and Kim, H.** (2018). Genome-wide association analyses  
654 identify new loci influencing intraocular pressure. *Hum Mol Genet* **27**, 2205-2213.

655 **Genetics of Glaucoma in People of African Descent, C., Hauser, M. A., Allingham, R. R., Aung, T., Van**  
656 **Der Heide, C. J., Taylor, K. D., Rotter, J. I., Wang, S. J., Bonnemaier, P. W. M., Williams, S. E. et al.** (2019).  
657 Association of Genetic Variants With Primary Open-Angle Glaucoma Among Individuals With African Ancestry.  
658 *JAMA* **322**, 1682-1691.

659 **Gharahkhani, P., Burdon, K. P., Cooke Bailey, J. N., Hewitt, A. W., Law, M. H., Pasquale, L. R., Kang, J.**  
660 **H., Haines, J. L., Souzeau, E., Zhou, T. et al.** (2018). Analysis combining correlated glaucoma traits identifies five  
661 new risk loci for open-angle glaucoma. *Sci Rep* **8**, 3124.

662 **Gould, D. B. and John, S. W.** (2002). Anterior segment dysgenesis and the developmental glaucomas are  
663 complex traits. *Hum Mol Genet* **11**, 1185-93.

664 **Gould, D. B., Smith, R. S. and John, S. W.** (2004). Anterior segment development relevant to glaucoma.  
665 *Int J Dev Biol* **48**, 1015-29.

666 **Gupta, R., Kumawat, B. L., Paliwal, P., Tandon, R., Sharma, N., Sen, S., Kashyap, S., Nag, T. C.,**  
667 **Vajpayee, R. B. and Sharma, A.** (2015). Association of ZEB1 and TCF4 rs613872 changes with late onset Fuchs  
668 endothelial corneal dystrophy in patients from northern India. *Mol Vis* **21**, 1252-60.

669 **Howell, G. R., Libby, R. T., Jakobs, T. C., Smith, R. S., Phalan, F. C., Barter, J. W., Barbay, J. M.,**  
670 **Marchant, J. K., Mahesh, N., Porciatti, V. et al.** (2007). Axons of retinal ganglion cells are insulted in the optic  
671 nerve early in DBA/2J glaucoma. *J Cell Biol* **179**, 1523-37.

672 **Howell, G. R., Soto, I., Zhu, X., Ryan, M., Macalinao, D. G., Sousa, G. L., Caddle, L. B., MacNicoll, K. H.,**  
673 **Barbay, J. M., Porciatti, V. et al.** (2012). Radiation treatment inhibits monocyte entry into the optic nerve head  
674 and prevents neuronal damage in a mouse model of glaucoma. *J Clin Invest* **122**, 1246-61.

675 **Isojima, T., Harita, Y., Furuyama, M., Sugawara, N., Ishizuka, K., Horita, S., Kajiho, Y., Miura, K.,**  
676 **Igarashi, T., Hattori, M. et al.** (2014). LMX1B mutation with residual transcriptional activity as a cause of isolated  
677 glomerulopathy. *Nephrol Dial Transplant* **29**, 81-8.

678 **Jeanne, M. and Gould, D. B.** (2017). Genotype-phenotype correlations in pathology caused by collagen  
679 type IV alpha 1 and 2 mutations. *Matrix Biol* **57-58**, 29-44.

680 **John, S. W., Hagaman, J. R., MacTaggart, T. E., Peng, L. and Smithes, O.** (1997). Intraocular pressure in  
681 inbred mouse strains. *Invest Ophthalmol Vis Sci* **38**, 249-53.

682 **John, S. W., Smith, R. S., Savinova, O. V., Hawes, N. L., Chang, B., Turnbull, D., Davisson, M., Roderick,**  
683 **T. H. and Heckenlively, J. R.** (1998). Essential iris atrophy, pigment dispersion, and glaucoma in DBA/2J mice.  
684 *Invest Ophthalmol Vis Sci* **39**, 951-62.

685 Keane, T. M., Goodstadt, L., Danecek, P., White, M. A., Wong, K., Yalcin, B., Heger, A., Agam, A., Slater,  
686 G., Goodson, M. et al. (2011). Mouse genomic variation and its effect on phenotypes and gene regulation.  
687 *Nature* **477**, 289-94.

688 Khawaja, A. P., Cooke Bailey, J. N., Wareham, N. J., Scott, R. A., Simcoe, M., Igo, R. P., Jr., Song, Y. E.,  
689 Wojciechowski, R., Cheng, C. Y., Khaw, P. T. et al. (2018). Genome-wide analyses identify 68 new loci associated  
690 with intraocular pressure and improve risk prediction for primary open-angle glaucoma. *Nat Genet* **50**, 778-782.

691 Knoers, N. V., Bongers, E. M., van Beersum, S. E., Lommen, E. J., van Bokhoven, H. and Hol, F. A.  
692 (2000). Nail-patella syndrome: identification of mutations in the LMX1B gene in Dutch families. *J Am Soc Nephrol*  
693 **11**, 1762-6.

694 Libby, R. T., Smith, R. S., Savinova, O. V., Zabaleta, A., Martin, J. E., Gonzalez, F. J. and John, S. W.  
695 (2003). Modification of ocular defects in mouse developmental glaucoma models by tyrosinase. *Science* **299**,  
696 1578-81.

697 Lichter, P. R., Richards, J. E., Downs, C. A., Stringham, H. M., Boehnke, M. and Farley, F. A. (1997).  
698 Cosegregation of open-angle glaucoma and the nail-patella syndrome. *Am J Ophthalmol* **124**, 506-15.

699 Liu, P. and Johnson, R. L. (2010). Lmx1b is required for murine trabecular meshwork formation and for  
700 maintenance of corneal transparency. *Dev Dyn* **239**, 2161-71.

701 Liu, Y., Peng, X., Tan, J., Darling, D. S., Kaplan, H. J. and Dean, D. C. (2008). Zeb1 mutant mice as a  
702 model of posterior corneal dystrophy. *Invest Ophthalmol Vis Sci* **49**, 1843-9.

703 MacGregor, S., Ong, J. S., An, J., Han, X., Zhou, T., Siggs, O. M., Law, M. H., Souzeau, E., Sharma, S.,  
704 Lynn, D. J. et al. (2018). Genome-wide association study of intraocular pressure uncovers new pathways to  
705 glaucoma. *Nat Genet* **50**, 1067-1071.

706 McIntosh, I., Dreyer, S. D., Clough, M. V., Dunston, J. A., Eyaid, W., Roig, C. M., Montgomery, T., Ala-  
707 Mello, S., Kaitila, I., Winterpacht, A. et al. (1998). Mutation analysis of LMX1B gene in nail-patella syndrome  
708 patients. *Am J Hum Genet* **63**, 1651-8.

709 McIntosh, I., Dunston, J. A., Liu, L., Hoover-Fong, J. E. and Sweeney, E. (2005). Nail patella syndrome  
710 revisited: 50 years after linkage. *Ann Hum Genet* **69**, 349-63.

711 McMahon, C., Gestri, G., Wilson, S. W. and Link, B. A. (2009). Lmx1b is essential for survival of  
712 periorbital mesenchymal cells and influences Fgf-mediated retinal patterning in zebrafish. *Dev Biol* **332**, 287-98.

713 Mimiwati, Z., Mackey, D. A., Craig, J. E., Mackinnon, J. R., Rait, J. L., Liebelt, J. E., Ayala-Lugo, R.,  
714 Vollrath, D. and Richards, J. E. (2006). Nail-patella syndrome and its association with glaucoma: a review of  
715 eight families. *Br J Ophthalmol* **90**, 1505-9.

716 Nair, K. S., Cosma, M., Raghupathy, N., Sellarole, M. A., Tolman, N. G., de Vries, W., Smith, R. S. and  
717 John, S. W. (2016). YBR/EIJ mice: a new model of glaucoma caused by genes on chromosomes 4 and 17. *Dis*  
718 *Model Mech* **9**, 863-71.

719 Pressman, C. L., Chen, H. and Johnson, R. L. (2000). LMX1B, a LIM homeodomain class transcription  
720 factor, is necessary for normal development of multiple tissues in the anterior segment of the murine eye.  
721 *Genesis* **26**, 15-25.

722 Quigley, H. A. and Broman, A. T. (2006). The number of people with glaucoma worldwide in 2010 and  
723 2020. *Br J Ophthalmol* **90**, 262-7.

724 Savinova, O. V., Sugiyama, F., Martin, J. E., Tomarev, S. I., Paigen, B. J., Smith, R. S. and John, S. W.  
725 (2001). Intraocular pressure in genetically distinct mice: an update and strain survey. *BMC Genet* **2**, 12.

726 Sawamura, H., Aihara, M. and Araie, M. (2014). Juvenile onset of ocular hypertension associated with  
727 de novo nail-patellar syndrome. *J Glaucoma* **23**, e122-5.

728 Shiga, Y., Akiyama, M., Nishiguchi, K. M., Sato, K., Shimozaawa, N., Takahashi, A., Momozawa, Y.,  
729 Hirata, M., Matsuda, K., Yamaji, T. et al. (2018). Genome-wide association study identifies seven novel  
730 susceptibility loci for primary open-angle glaucoma. *Hum Mol Genet* **27**, 1486-1496.

731 Smith, R. S., Roderick, T. H. and Sundberg, J. P. (1994). Microphthalmia and associated abnormalities in  
732 inbred black mice. *Lab Anim Sci* **44**, 551-60.

733 **Spitalny, L. A. and Fenske, H. D.** (1970). Hereditary osteo-onychodysplasia. *Am J Ophthalmol* **70**, 604-8.

734 **Sulik, K. K., Johnston, M. C. and Webb, M. A.** (1981). Fetal alcohol syndrome: embryogenesis in a mouse

735 model. *Science* **214**, 936-8.

736 **Sweeney, E., Fryer, A., Mountford, R., Green, A. and McIntosh, I.** (2003). Nail patella syndrome: a

737 review of the phenotype aided by developmental biology. *J Med Genet* **40**, 153-62.

738 **Taylor, K. D., Guo, X., Zangwill, L. M., Liebmann, J. M., Girkin, C. A., Feldman, R. M., Dubiner, H., Hai,**

739 **Y., Samuels, B. C., Panarelli, J. F. et al.** (2019). Genetic Architecture of Primary Open-Angle Glaucoma in

740 Individuals of African Descent: The African Descent and Glaucoma Evaluation Study III. *Ophthalmology* **126**, 38-

741 48.

742 **Thaung, C., West, K., Clark, B. J., McKie, L., Morgan, J. E., Arnold, K., Nolan, P. M., Peters, J., Hunter, A.**

743 **J., Brown, S. D. et al.** (2002). Novel ENU-induced eye mutations in the mouse: models for human eye disease.

744 *Hum Mol Genet* **11**, 755-67.

745 **Vishal, M., Sharma, A., Kaurani, L., Alfano, G., Mookherjee, S., Narta, K., Agrawal, J., Bhattacharya, I.,**

746 **Roychoudhury, S., Ray, J. et al.** (2016). Genetic association and stress mediated down-regulation in trabecular

747 meshwork implicates MPP7 as a novel candidate gene in primary open angle glaucoma. *BMC Med Genomics* **9**,

748 15.

749 **Vollrath, D., Jaramillo-Babb, V. L., Clough, M. V., McIntosh, I., Scott, K. M., Lichter, P. R. and Richards,**

750 **J. E.** (1998). Loss-of-function mutations in the LIM-homeodomain gene, LMX1B, in nail-patella syndrome. *Hum*

751 *Mol Genet* **7**, 1091-8.

752 **Webster, W. S., Walsh, D. A., McEwen, S. E. and Lipson, A. H.** (1983). Some teratogenic properties of

753 ethanol and acetaldehyde in C57BL/6J mice: implications for the study of the fetal alcohol syndrome. *Teratology*

754 **27**, 231-43.

755 **Weinreb, R. N., Aung, T. and Medeiros, F. A.** (2014). The pathophysiology and treatment of glaucoma: a

756 review. *JAMA* **311**, 1901-11.

757 **Wever, I., Largo-Barrientos, P., Hoekstra, E. J. and Smidt, M. P.** (2019). Lmx1b Influences Correct Post-

758 mitotic Coding of Mesodiencephalic Dopaminergic Neurons. *Front Mol Neurosci* **12**, 62.

759 **Williams, P. A., Harder, J. M., Foxworth, N. E., Cochran, K. E., Philip, V. M., Porciatti, V., Smithies, O.**

760 **and John, S. W.** (2017). Vitamin B3 modulates mitochondrial vulnerability and prevents glaucoma in aged mice.

761 *Science* **355**, 756-760.

762 **Yokoyama, T., Silversides, D. W., Waymire, K. G., Kwon, B. S., Takeuchi, T. and Overbeek, P. A.** (1990).

763 Conserved cysteine to serine mutation in tyrosinase is responsible for the classical albino mutation in laboratory

764 mice. *Nucleic Acids Res* **18**, 7293-8.

765 **Youngblood, H., Hauser, M. A. and Liu, Y.** (2019). Update on the genetics of primary open-angle

766 glaucoma. *Exp Eye Res* **188**, 107795.